Toward in-cylinder absorption tomography in a production engine

Towards In-Cylinder Absorption Tomography in a Production Engine

Paul Wright[1], Charles A. Garcia-Stewart[1], Stephen J. Carey[1], Francis P. Hindle[1]*, Stephen H. Pegrum[2], Stephen M. Colbourne[2], Paul J. Turner[2], William J. Hurr[2], Tim J. Litt[3], Stuart C. Murray[3], Sam D. Crossley[3], Krikor B. Ozanyan[1] & Hugh McCann[1]

[1]School of Electrical & Electronic Engineering, University of Manchester, UK

*(now at Laboratoire de Physico-Chimie de l'Atmosphère, Université du Littoral Côte d'Opale, Dunkirk, France)

[2]Roush Technologies Ltd., Brentwood, UK

[3]AOS Technology Ltd., Melton Mowbray, UK

Design requirements for an 8000 frame/second dual-wavelength ratiometric chemical species tomography system, intended for hydrocarbon vapor imaging in one cylinder of a standard automobile engine, are examined. The design process is guided by a wide range of spectroscopic measurements on iso-octane and comprehensive results from laboratory phantoms and research engines, including new results on temporal resolution performance. Novel image reconstruction techniques, necessary for this application, are presented. Recent progress towards implementation, including details of the optical access arrangement employed and signal to noise issues, is described.

We also present first cross-cylinder IR absorption measurements from a reduced channel-count (non-tomographic) system and discuss the prospects for imaging.

OCIS codes 100.6950, 110.3080, 120.1740, 300.6260

1. Introduction

For some years, members of the Manchester (formerly UMIST) Industrial Process Tomography group and their collaborators have been working towards the use of optical tomography, based on near-infrared absorption by hydrocarbons (HC), as a diagnostic technique for studies of air-fuel mixture preparation within vehicle engines. This work has been motivated, in part, by the potential of the technique to address pressing problems in automotive combustion but also affords an excellent opportunity to demonstrate the first robust and portable implementation of chemical species tomography (CST), for the study of flowing and reacting industrial processes. Other authors (e.g. Santoro *et al*[1]) indicated the promise of CST, typically by scanning a single-channel measurement system across a suitable subject, but further engineering research was required to turn such demonstrations of principle into practical instrumentation.[2,3] More recently, CST has been applied to laboratory studies of chemical process techniques.[4] In this paper we present our own efforts to develop tomographic imaging of HC distributions for application to internal combustion (IC) engines, from proof-of-principle to recent progress on implementation within a production engine. Successful imaging in an IC engine requires both chemical selectivity and very high temporal resolution (~ 10^4 frames / second [fps]). CST can discriminate between HC and other species present and, thanks to modern photonics, electronics and computing technology, it can also offer the temporal performance

required for the study of flow and mixing processes occurring within the combustion chamber.

Early work was restricted to laboratory phantoms and single-cylinder research engines. Recently, significant steps have been taken towards performing optical absorption tomography within an otherwise standard multi-cylinder IC engine mounted on a dynamometer, as part of a research program known as IMAGER. The integration of this type of measurement system into a vehicle engine presents significant challenges in both optoelectronic engineering and tomography but, given the vast number of such engines in use globally, even small performance improvements are potentially of great benefit. Unlike research engine studies, the IMAGER program is not restricted to providing insight into fuelling and combustion processes in a generic sense; it is also intended to provide a diagnostic tool to enhance engine calibration, which should therefore contribute more directly to the reduction of emissions and fuel consumption.

The majority of the group's work on HC-imaging to date has exploited the wide and relatively unstructured absorption feature that all partially or fully saturated hydrocarbons display at 1700 nm; this results from the first overtone of the fundamental C-H stretch absorption and various combinations that arise due to differing bonding configurations of the carbon atoms in the molecule.[5] This feature offers sensitivity to a wide range of HC species, making it a good choice for studies involving multi-component fuels, such as unleaded gasoline (ULG). Although the absorption from this feature is weaker by about two orders of magnitude than that from fundamental lines in the mid-infrared, limiting its usefulness for the measurement of low concentrations, it is well suited to the imaging of *near-stoichiometric* air-gasoline mixtures. Under typical operating conditions, for which

the product of concentration and path length is ~10^3 ppm·m, absorption of around 5% is expected across a cylinder diameter at 1700 nm. Mid-IR (3.4 μm) absorption under these conditions would be so strong that it may actually be detrimental to the measurement; in effect the fuel-vapor plume would become too opaque for effective CST. Near-infrared operation can also have significant advantages in terms of source performance, room-temperature operation, and the availability of optical fibers and related components. Several authors[5,6,7] have considered the relative merits of sensor operation in each of these spectral regions but the reader is particularly directed to the review by Allen.[8]

In our system, a second (reference) wavelength, chosen to exhibit minimal specific absorption by any of the reactants or products in the combustion chamber, is deployed so that the effects of attenuation mechanisms not specific to hydrocarbons can be taken into account. We have already presented the theory underlying this dual wavelength ratiometric (DWR) approach in earlier publications[2,3] for the specific case of HC absorption at 1700 nm. For the purposes of our discussion here, we recall the following basic relationships and definitions: The photodetector-received intensity $I_r(\lambda)$, at wavelength λ, that is transmitted over a path L through a gaseous cloud containing a target species of *spatially varying* concentration c, is given by :

$$I_r(\lambda) = I_O(\lambda)\exp\left(-k(\lambda)\int_L c\,.dl\right) \tag{1}$$

where $I_o(\lambda)$ is the incident intensity, $k(\lambda)$ is the wavelength-dependent absorption coefficient for the target species and dl is the line element. The line integral in equ. (1), termed the *path-concentration integral* (PCI), is the quantity that we need to determine in order to carry out tomographic reconstruction of the concentration distribution c; it is readily obtained from the ratio of transmission of an absorbed wavelength to that of a non-specifically absorbed (reference) wavelength (equ. 2).

$$\int_{L} c\,.dl = \frac{1}{k(\lambda_1)-k(\lambda_2)} \ln\left(\frac{I_r(\lambda_2)}{I_r(\lambda_1)}.\frac{I_O(\lambda_1)}{I_O(\lambda_2)}\right) \quad (2)$$

Simultaneous measurement of the transmitted intensity at each of the two wavelengths is performed using a dual-frequency lock-in technique, described extensively elsewhere.[2,3]

The breadth of the absorption feature in question (≈ 55 nm for 3 bar, 150ºC, 0.0073 mol/liter iso-octane) is very large compared to the range of emission wavelength commonly available from current tuning of a diode laser. Such broad tuning ranges are attainable using *external cavity* diode lasers but the tuning bandwidth of these devices is insufficient for our needs. Consequently, two separate DFB laser sources are used to implement the measurement, rather than wavelength scanning a single device in the manner typical of differential absorption spectroscopy (DAS) or TDLAS systems.

Although chemical species tomography of other gas phase processes has been demonstrated using bulk optics[4], we believe that fiber optics currently offer the best prospects for system implementation, subject to the space constraints presented by a multi-cylinder vehicle engine. Their use does, however, introduce additional problems, as discussed in Section 3.3. The proximity of the absorption feature of interest to the optical telecommunications bands does, at least, ensure that a wider range of fibers and related devices is available, and at lower cost, than would be the case in the mid-infrared. Given that a 32-channel tomograph is likely to use more than 500 m of fiber, the substantially higher cost of mid-IR products is a significant factor.

The authors are unaware of any existing study presenting line-of-sight infrared absorption measurements across the combustion chamber of a *production* engine, although such results have been reported for single-cylinder, transparent-walled,

research engines.[9,10] Philipp *et al*[11] applied a form of 'passive' optical tomography (i.e. based upon broadband thermal and chemiluminescent emission) to the imaging of flame fronts, using optical fibers and microlenses embedded in an engine gasket. This technique is not chemically selective and is rather less demanding, in optical engineering terms, than systems, such as our own, which require alignment to be maintained between the launch and receive optics.

This paper will show that all key requirements for tomographic imaging of hydrocarbon distributions have been met, including bench-top demonstrations of the technique, before considering the particular difficulties arising from operation in the production engine environment. The latter will be shown to exert significant influence upon not only the hardware design but also the approach that must be taken to tomographic reconstruction. Section 2 summarizes the various laboratory and research engine trials that provide the foundation for our present program, including new material that substantially extends our previously published results. In Section 3 we describe recent progress towards the application of tomography in one cylinder of a production automobile engine. Within this latter program, most effort, to date, has been directed at achieving the required performance from individual measurement paths. A reduced channel-count system, featuring only three beam-paths, has been operated successfully in a running engine; initial results from these tests are presented. We conclude with a discussion of the prospects for implementation of a tomography system, of around 30 channels, within this same engine.

2. Laboratory Phantom & Research Engine Studies

2.1 Characterization of the absorption feature

In the absence of existing literature on the gas-phase absorption properties of either ULG or iso-octane, the latter being a commonly used reference fuel, characterization of the absorption feature under conditions of interest was a priority. Initial measurements, using a broadband source and monochromator, revealed the general form of the absorption spectrum and its variation with temperature and pressure.[2,3] Figure 1(a) shows the significant effect of pressure, over a range typical of engine compression, on the transmission of iso-octane in air (0.0073 mole/liter; 164 mm path length) at 150°C. At 1700 nm, the absorption coefficient of a stoichiometric mixture (10 bar, 80ºC) was found to be (84 ± 11) L mol^{-1} m^{-1}. Further measurements showed that the absorption coefficient did not vary appreciably over the range of concentration (0.2 to 15 times stoichiometry) anticipated in the combustion chamber.[12] The absence of any significant fine structure in the region 1699.4 to 1700.4 nm was then confirmed using a tunable diode laser source of linewidth 1.5 MHz.[12] Although most of this work was carried out using the reference fuel iso-octane to achieve repeatability, some tests were duplicated with ULG to establish the wider applicability of the results. Absorption data for gasoline have subsequently appeared in a publication by McNesby *et al*[5] but variation with temperature and pressure were not studied. They found the C-H stretch first-overtone absorption coefficient (at 1.7 μm) for middle-distillate fuel vapors (1 bar, 21ºC) to be approximately (163 ± 24) L mol^{-1} m^{-1}, which is similar to the figure we obtain for iso-octane at that same pressure, but 80ºC, of (127 ± 12) L mol^{-1} m^{-1}.

Calculations[2,12] using the HITRAN database[13] yielded candidate reference wavelengths where there is no significant specific absorption by relevant species such as O_2, H_2O, CO, CO_2, NO, OH, CH_4. In the early work reported previously[2,3], a reference wavelength was supplied by a telecoms diode laser, at 1546nm (nominally

1550nm). The DWR technique, implemented with these two DFB laser sources, was then calibrated for pressure and temperature variation, as shown in Figure 1(b). Corresponding monochromator-based data are shown for comparison; the laser-based data are seen to be less variable with temperature, which we attribute to greater simplicity of the overall measurement procedure in this case. The temperature-insensitivity of the absorption measured by the laser-based DWR technique is of central importance to its application for tomographic imaging within an engine, and its variation with pressure is sufficiently smooth to allow straightforward calibration using measured cylinder pressure.

2.2 Tomographic imaging from single-channel measurements of gas plumes

Mechanical scanning of a single-channel measurement system across a 5.5 mm diameter laminar gas plume (70% butane / 30% propane) provided data from four tomographic projections (angles of observation), each containing 33 measurement paths.[3] Images generated using the algebraic reconstruction technique (ART)[14,15] showed good localization of the plume, although a few artefacts were evident close to the edges of the measurement space. This study demonstrated the viability of HC imaging using absorption at 1700 nm. Careful examination of the individual measurements does, however, reveal some interesting effects, which have implications for our present system design. Most notably, apparently negative absorption values are observed near to the edges of the plume. These have been attributed to wavelength dependent changes in the optical coupling efficiency between transmitter and receiver, resulting from refractive index variations in the measurement space. Such variations may occur between regions of dissimilar density, temperature

or composition. The effect is compounded by the inevitable disparity in the (Gaussian) launch profiles of the 1550 nm and 1700 nm beams. In other ratiometric optical measurement systems, e.g. two-color optical pyrometry, great care is often required to achromatize the optical system sufficiently to ensure the validity of the ratio. In the present case, it is similarly important that the two wavelengths take closely-matched paths through the measurement space but, even given otherwise perfectly achromatic optics, it is not possible to control or predict the effect of the *measurement subject* itself; some level of refractive-index dispersion or wavelength-dependent scattering may be present. A general improvement can be effected by reducing the separation of the measurement and reference wavelengths, and so decreasing both the relative refractive index variations and the degree of launch mismatch; the new tomography system resulting from the IMAGER program will employ a reference wavelength (1651 nm) much nearer to 1700 nm than the 1550 nm used previously. Closer spacing than this is undesirable as the reference beam will itself show appreciable absorption by HC, as shown by our measurements of ULG absorption spectra.[12]

2.3 8-channel studies on a research engine

Having demonstrated the basic viability of HC imaging, the next requirement was to establish that reliable PCI estimates could be obtained across the combustion chamber of an engine. Tests conducted on a single-cylinder, 'glass-walled', gasoline direct injection (GDI) research engine provided an early insight into some of the problems to be faced. Eight measurement paths were monitored during both homogenous and stratified charge operation of the engine. The beam paths were chosen to encompass a variety of in-cylinder conditions; both diametric and non-diametric beams were included, in various positions with respect to the valves. Some results from this study

have been published previously[16] but others are of great significance in the design of the new system. Firstly, analysis of the attenuation signal during the *initial* stages of a fuel injection event showed significant content at frequencies as high as 100 kHz (intake stroke, 49-98º after top-dead-centre [TDC]). This is greater than the separation of the laser modulation frequencies in our first-generation tomograph, making accurate demodulation impossible during this period. The high levels of scattering associated with spray events will always present a severe challenge to DWR-based imaging. Nevertheless, the facility to use higher carrier frequencies than previously is clearly desirable as this will expand the range of conditions that can be imaged, particularly in the case of GDI engines. Secondly, the tests confirmed the effectiveness of the DWR technique in dealing with unwanted sources of cross-cylinder attenuation, such as soot particles, as indicated by the performance achieved.[16] Absorption levels of around 0.5% could be resolved within a single cycle, which compares favorably with the expected peak absorption of 4-5%. Most encouragingly, no evidence was found to suggest that in-cylinder application of the technique would not be possible. A more complete discussion of these tests, with statistical analyses, can be found in Carey.[12]

2.4 32-channel studies on a laboratory phantom

Hydrocarbon imaging was carried out in a laboratory simulator of an engine cylinder, to demonstrate the available spatial and temporal resolution of our first-generation tomography system, and partially reported by Hindle *et al*.[3,16] A schematic overview of this system is given in Figure 2. The measurement space was a section across a silica-walled pressure vessel, into which either gaseous propane or liquid gasoline could be injected (Fig. 3). The vessel also includes facilities for heating, pressurization and purging of its contents; details of optics and electronics are

presented in reference 3. This arrangement allows the creation of approximately known spatial and temporal HC distributions for test purposes. In common with other forms of imaging, such targets are referred to as 'phantoms'. As compared to the gas-plume tests described in Section 2.2, this study utilized a number and distribution of measurement paths much closer to what was considered to be possible in a combustion chamber (four projections, each of eight parallel beams) in order that the performance obtained would be indicative of the system's potential.

Previously published results obtained from gaseous propane tests include imaging of a single 20 ms injection event, and of two spatially and temporally separated injections, each of 10 ms duration; the spatial separation was 36% of the vessel diameter, and the temporal separation was 100 ms.[3] The practical difficulties of implementing gas-phase phantoms mean that these results are, in some respects, qualitative as the actual form of the object is quantitatively unknown. Nevertheless, they provide a useful demonstration of both the spatial and temporal resolution of the system. Section 3 discusses further developments in image reconstruction techniques for the gaseous injection case, and presents new images obtained.

Imaging of fuel sprays from a GDI injector was also carried out.[16] In this latter case, image reconstruction of the HC vapor distribution, based upon PCI's calculated from DWR measurements, was only possible once sufficient vaporization had occurred. An alternative approach was developed, for use immediately after start of injection, in which attenuation of the 1550 nm reference beam was used to map the distribution of scattering processes within the measurement space. Fuel droplets will be the principal cause of such scattering so this offers a means to perform spray imaging using a subset of the hardware employed for DWR imaging of HC absorption. The injector provides a rapidly varying fuel distribution of known basic

form (conical) against which the system's output can be compared. The resulting images were found to agree well with photographic observations of the injector's spray cone. Time-resolved imaging of an iso-octane injection, at three heights within the chamber, showed the system to have the temporal performance necessary for the imaging of spray features (Figure 4).

Initial analysis[3,16] of these first tests indicated that DWR-based imaging of hydrocarbon vapor distributions, with spatial resolution of around 20% of the cylinder diameter, was practicable at rates around 1000 fps, using this first generation system. Subsequent further analysis, in conjunction with refinement of the reconstruction process (see 3.1 below) has shown reliable image reconstruction at a rate of 3500 fps. Even this latter rate is probably too low for useful application to a production engine as it equates to one frame for each engine rotation interval of 7° of crank angle (CA) at 4000 rpm; frame rates around 8000 fps (i.e. one frame per 3° CA at 4000 rpm), or higher, are considered to be desirable but will require improved signal-to-noise performance.

3. Integration Into a Production Engine - IMAGER

From the preceding material, three main areas where improvements can be made to enhance the prospects for tomography within a production engine are apparent: Reduced wavelength separation of the laser sources; increased and more widely spaced modulation rates; and improved signal-to-noise performance. The second-generation near-infrared absorption tomography system, currently being built as part of the IMAGER program, aims to address these issues as well as others demanded by the transfer to a 'real' engine environment.

Space constraints within the engine are severe. The 4-cylinder, 2.0 liter target engine has a cylinder wall circumference of less than 280 mm and not all of this can

be utilized, most obviously the portion bordering the adjacent cylinder. In practice, we expect to accommodate around 30 beams, each requiring a pair of collimators, necessitating an extremely compact design. The combustion chambers are not the only voids within the engine block; various coolant channels and other passages are present, whose locations preclude the use of a regular array of measurement beams. Tomographic reconstruction from the resulting severely under-determined datasets, measured from an irregular beam array, is not a well-established technique and has required additional effort (Section 3.1). Good optical access to the combustion chamber is vital to the IMAGER program but the environment is extremely harsh; the optics will be subjected to pressures that rise from partial vacuum to 30 bar in a few milliseconds, as well as flame impingement and the chemical effects of the fuel and its combustion products. Engine blocks are known to exhibit cyclic flexing and vibration during operation, which has implications for collimator alignment. The optical concept developed for IMAGER uses a structure referred to as the **OP**tical **A**ccess **L**ayer (OPAL), which houses and protects the collimation optics and fibers used to transfer light to and from the combustion chamber. This is described in Section 3.2. Signal-to-noise issues and changes in the optoelectronic design are discussed in Section 3.3. Example results obtained in a pilot study, using a reduced channel-count system, are presented in Section 3.4. Present efforts to extend the work described here to provide full coverage of the cylinder cross-section, and thus permit tomographic imaging of the HC distribution, are discussed in Section 3.5.

3.1 Tomographic reconstruction from limited and irregular measurement arrays

With few exceptions, hard-field (see Section 4) tomographic reconstruction is performed from measurements that, in some sense, sample the measurement subject in a uniform manner. Measurement paths are usually arranged so as to provide data in several 'projections', each consisting of measurements made along a number of individual paths that are usually related to one another by either a linear or angular translation by a fixed increment; the latter type is usually referred to as a 'fan-beam' arrangement. The projections themselves are usually equally spaced, in angular terms. Measurement data are often presented as a sinogram, showing their variation in a cylindrical polar coordinate system. The quantity of data is often very large; clinical X-ray CT scans typically employ $10^5 – 10^6$ individual path attenuation measurements. The fundamentals of image reconstruction for this case are presented in Bertero & Boccacci.[17] However, application of IR absorption tomography to a production engine dictates that the available PCI measurements will be both limited in number and sampled from an irregular spatial array of beam paths. The early bench-top work discussed in Section 2, with a regular array of beams, has served to illuminate the issues that arise as a result of having a *small number* of beams, and new results from that work are included below. We are currently addressing the issue of *irregular* arrays and our earliest findings in this area are also presented.

Various authors have examined limited-data tomography, albeit for less severely restricted datasets than are expected from our present work.[18,19,20,21] In general, the inclusion of some form of *a priori* knowledge is helpful in rendering the problem more tractable. In our particular case, the HC concentration distribution can be constrained to be non-negative and smoothly varying. The first of these clearly has a sound and simple physical basis, but the second merits careful consideration: It can be justified on the basis that the inherently limited spatial resolution of the data (≈

D/5, where *D* is the diameter of the cylinder) prevents accurate imaging of 'sharp' features (i.e. those with high spatial frequency content) so this constraint need not detract from the system's imaging performance; more fundamentally, for purely gas-phase processes, it is a reasonable expectation in most cases that the concentration distributions of various species will vary smoothly in space. Of course, it is possible to conceive of circumstances where the latter *a priori* expectation is invalid, and the value of performing tomographic measurements with small numbers of beams in such applications must then be reviewed carefully. This highlights the necessity of performing modeling/simulation before building a system, then calibrating its performance in the expected parameter envelope. We have chosen, for the time being, to focus on the 'smooth problem', and it is necessary to test the system performance on appropriate phantoms. In effect, we are aiming to generate an HC distribution image, devoid of high spatial frequencies, which can account for the observed measurement data. In our first exploration of this problem, we applied two approaches of this type to the reconstruction of both simulated and measured data with encouraging results.[22]

In the first publication[3] of these demonstrator results, the so-called Algebraic Reconstruction Technique (ART)[14,] was used in iterative form. ART was initially developed for X-ray CT and electron microscopy.[15] In our case, with only 32 measurements, the use of ART is not optimal. [Although, we note that various authors in X-ray CT for industrial processes are continuing to develop it for moderately small numbers of measurements (100 – 1000).[23]] Hence, we have recently developed more appropriate multi-step algorithms based on the Landweber iterative technique,[24,25] which we explain briefly here: *Step 1* - an initial estimate is found by applying the simple linear back projection (LBP) technique,[14] viz. $\mathbf{g}_1(x,y)=\mathbf{S}^T\mathbf{p}$, where $\mathbf{g}$ is the

estimate of the true concentration distribution vector **c** and is a vector representing the concentration in each of *N* pixels, **p** is the vector of *M* measurements of PCI, and $\mathbf{S}^T$ is the *N* x *M* transpose of the sensitivity matrix **S** and is used here as an approximation to $\mathbf{S}^{-1}$. The definition of **S** is that, for a given **c**, the measurement vector **p** is given by **p=Sc**; *Step 2* - the Landweber technique repeatedly compares the original measurements with those that would be expected with the updated estimate $\mathbf{g}_k$ of concentration distribution, viz. $\mathbf{Sg}_k$. The discrepancy is fed into the LBP process to create an 'error image' and this is multiplied by a 'relaxation constant' denoted α; the scaled error image is added to the previous estimate to generate a new estimate $\mathbf{g}_{k+1}$; *Step 3* – any negative elements of $\mathbf{g}_{k+1}$ are returned to zero; *Step 4* - the new image is compared with the previous estimate for convergence, compared with some pre-set criterion. Mathematically, the first three steps of this process are written as:

$$\mathbf{g_{k+1}} = f\left[\, \mathbf{g_k} + \alpha \mathbf{S}^T\left(\mathbf{p} - \mathbf{S}\mathbf{g_k}\right) \,\right] \tag{3}$$

where *f* is the operator which ensures non-negativity and, in our case, applies a smoothing filter.

We begin by addressing the reconstruction of measured data from the 32-channel bench-top system described in Section 2.4. In this case, we have interpolated the measured data in both directions within the sinogram (using spline fits), i.e. in linear space within projections and in angular space between projections. In all, the 32 real measurements for each image were used to generate a 'dataset' of 3600 'measurements'. These were then used in the above Landweber procedure. The same interpolation was done with the 'error' vector ($\mathbf{p} - \mathbf{Sg_k}$) at subsequent stages of the iteration. For this relatively large number of interpolated 'data' it is generally preferable to use the well-known procedure of filtered back projection (FBP),[17] rather than LBP. This helps to remove the non-zero background that typically results from

the use of LBP. Sample images are shown in Fig. 5(a) for injection of a single propane jet (at location A) and in Fig. 5(b) for a dual injection with a temporal offset (A then B). Figs. 5(a) and 5(b) were produced from raw frame data that were recorded at 17000 samples/s and then averaged at 5 samples per frame in software, to produce a frame rate of 3500 fps. Image reconstruction was then performed by the technique described above. The color scale on these images is not calibrated to an absolute scale of concentration; it is the variation of concentration within the imaged cross-section, and from frame to frame, that is significant. The data for the images in Fig. 5(a) were measured at a depth of 10 mm below the injector outlet, and the injection pulse lasted 10 ms. The early reconstructed images (frames 1 & 2; 30.6 ms, 51.2 ms after start of injection) show a growth in concentration directly below the injection point. This is followed by a reduction as the propane jet mixes with air within the chamber (frames 3 & 4; 98.5 ms, 145.0 ms).

The images in Fig. 5(b) show examples of the distribution arising from a dual propane injection sequence, each injection lasting 10 ms, separated in both space (30 mm) and time (100 ms). Just as in the single injection case, the measurement plane is 10 mm below the injector outlets. Below injector location A, the concentration of propane in the image plane first rises (frame 1; 28.8 ms) and then falls (frame 2; 98.8 ms), as expected. The concentration rises under injector B after the start of the second injection (frame 3; 136.5 ms) but an almost immediate increase is also seen under injector A (frame 4; 145.0 ms), unlike in Fig. 5(a). The distribution then varies rapidly for a period before starting to settle to a homogeneous mixture. These events can be understood as the ‘collision’ of two counter-flowing gas jets, one (from injector B) having a higher energy density than the other (from injector A) at the time of collision.

The spatial aspects of the images in Figs. 5(a) and 5(b) serve to show the general validity of the tomography system in terms of both hardware and software, even if the concentration values require further quantification. They also illustrate the excellent temporal resolution of the technique and its potential to 'follow' individual fuel injections into an engine cylinder, albeit restricted to a single plane in the present case and still with sub-optimal temporal resolution. A number of artefacts do remain to be addressed, such as the obvious 'angular smearing' of the images, and the unexpectedly low concentration values between the fuel-rich zones and the edge of the chamber. In these respects, however, it is important to bear in mind the fundamental limits on spatial resolution in this system, viz. about $D/5$ (17 mm) in linear terms, or around 4% in area.

The design of a practical optical access arrangement for a production engine is discussed in Section 3.2. The beam array is necessarily irregular, and an early attempt to design such an array is shown in Figure 6. This is a relatively unusual problem for tomographic image reconstruction. Our present approach is to use the Landweber technique, but with a different means of introducing smoothing. The technique is implemented as described in equation 3, with the exception that the output of the LBP is processed further: A sparse matrix of image data at the *beam crossing points* is extracted and subjected to a 2-D interpolation and smoothing process to generate an image over the whole image space. For the beam array in Fig. 6, we have examined the performance of this algorithm for a number of simulated phantoms, and example results are shown in Fig. 7. Simulated reconstruction offers an efficient means to test the effectiveness of the reconstruction strategy and the candidate measurement grid, for a range of object distributions. The simulated phantoms used here, with sharp contrasts in target gas concentration, cannot be reconstructed accurately, given the

smoothness assumption incorporated within the algorithm. The reconstructed images in Fig. 7 illustrate some limitations of this particular beam array: The two phantoms in Fig. 7 are identical, apart from a rotation of 45º, but the reconstructed images are very different, particularly in the separation of the two regions of high concentration.

Earlier reconstructions of uniformly-sampled data using ART without interpolation, such as those in Figure 4, show strong effects of the underlying measurement paths, with step changes in concentration between geometric regions defined by the beam layout. This is physically unrealistic and may hinder interpretation of the images. Although these artefacts could be removed by post-processing the reconstructed image using a low-pass spatial filter, the inclusion of the smoothness constraint within the iterative algorithm offers a more logical route to achieving an estimate of the true concentration distribution c, consistent with limited observed data $\mathbf{p}$.

3.2 The OPAL concept

Unlike the 'optical gasket' arrangement used by Philipp *et al*,[11] the OPAL is a substantial structure that replaces the uppermost portion of the engine block, including not just part of the cylinder wall but also appropriate sections of the various coolant channels, etc., whilst preserving the chamber geometry; in particular, the compression ratio is unchanged. This permits the optical paths to be defined and tested during OPAL assembly, before being transferred to the engine. Nevertheless, there are many constraints on the fiber routing through the OPAL assembly, and the part of the cylinder perimeter that is available for launch and receive optics is limited. There are various candidate arrangements for beam paths across the cylinder, one of which has been illustrated in Figure 6. The final choice of beam arrangement is informed by assessments of image quality, as illustrated in Figure 7. This optimization process

involves detailed input from optical design, engine technology and image reconstruction.

The 3-channel OPAL used for initial tests within the target engine is shown in Figure 8. Optical fibers enter the OPAL at three points around its perimeter, before running through machined grooves to the collimator assemblies that define the launch and receive geometries. Further discussion of the work carried out using this 3-channel OPAL will appear in Wright *et al*.[26]

3.3 Optoelectronic design

Effecting an improvement in signal to noise ratio (SNR) was a high priority in the design of IMAGER since, despite our desire to raise the imaging rate, no increase in the available optical power was anticipated. Although the (near-stoichiometric) species concentration is high, relative to many gas sensing applications, other factors make achieving the SNR necessary for accurate imaging a demanding task. *1) Available power:* The modest output (< 5 mW) of the 1651 nm and 1700 nm laser diodes must be divided among the measurement beams; allowing for losses, the received optical power at each detector is expected to be less than 10 μW, which is two orders of magnitude less than in many near-IR laser diode gas sensors. *2) Absorption:* The cross-cylinder path lengths are short, typically 80 mm, and the HC absorption coefficient at 1700 nm is comparatively low (as discussed in Section 1). HC-induced absorption is typically less than 5%, despite the relatively high concentration of HC. *3) Hardware architecture:* Various harmonic detection techniques are typically employed for sensitivity enhancement in near-IR diode laser spectroscopy[7] but these cannot be implemented within the DWR approach as no significant wavelength-dependent change will occur across the current tuning range of

either source. *4) Speed of measurement:* Considerable bandwidth (~ 10^4 Hz) is necessary to meet the temporal resolution requirement.

The greatest opportunity to enhance SNR within the *electronic* hardware was felt to lie in optimization of the photodiode receiver design. An improvement of around 20 dB in the measured SNR at the receiver has been achieved, giving a noise density (measured at 440 kHz) of less than 2 $\mu V \cdot Hz^{-0.5}$ at the receiver output.[27] This amendment also extended the operating bandwidth of the receiver sufficiently to support operation at modulation frequencies up to 500 kHz. Lock-in amplification limits noise bandwidths appropriately and a digital interface to the data storage PC minimizes the risk of signal corruption by interference. Little scope is thought to exist for further noise reduction in the signal recovery path.

Several forms of *optical noise* will inevitably be present in any system of this type. This can be especially problematic as, unlike electronic noise, these processes are often independent of signal level; SNR will therefore improve with increasing optical power only until such optical noise processes become dominant. In a recent review of fiber-optic sensing, Kirkendall & Dandridge[28] discuss a similar balance between fiber-derived and electronic noise, for an interferometric sensor; in their example the transition occurs at around 5 μW. In our case, the exact location of this transition depends upon the bandwidth selected for signal recovery but, following the electronics improvements mentioned above, optical noise has become the most significant problem under some operating conditions. Understanding the origins of such noise can be helpful in its reduction.

Source amplitude noise is a property of the particular laser employed but can, in principle at least, be cancelled using balanced detection schemes. However, these are hard to implement in practice, due to the difficulties of achieving adequate

channel balance,[8] and are not readily incorporated within our current DWR architecture. At present, interferometric and fiber effects are of greater concern. The combustion chamber and each pair of collimator optics form a low-finesse Fabry-Perot etalon and other similar, but weaker, interferences are present, due to reflections from connectors and other discontinuities. The output intensity, in transmission mode, from a weak etalon bounding a low-absorption gas path can be described by[29]

$$\frac{I_T}{I_{IN}} \approx \beta \left\{ \left[1-\gamma \right] + 2\beta r_1 r_2 \cos\left(2\pi\upsilon\tau\right) \right\} \tag{4}$$

where I_T and I_{IN} represent the transmitted and input intensities respectively, β the (intensity) coupling efficiency across the etalon, γ the fractional absorption along the path, r_1 and r_2 the reflectivities of the bounding surfaces, υ the source frequency, and τ the round trip time for the etalon ($2d/u$, where d is the path length and u the speed of light in the medium). The final term represents the unwanted interference. By inspection, we can identify three obvious approaches to its suppression. Firstly, the coupling efficiency β appears at higher order in the unwanted term than in the absorption signal; decreased coupling will therefore favor the latter. If taken to excess, such reduction of coupling efficiency will, of course, ultimately lead to *decreased* SNR, as electronic noise regains prominence. The most likely cause of a reduction in β is imperfect collimation, which is expected to occur to some extent as a result of contamination of the optical surfaces within the combustion chamber. Similarly, reduction of the reflectivity of either bounding surface, as may be achieved using dielectric coatings, will also act to reduce the relative strength of any etalon contribution. The durability of such coatings in a running engine is likely to be very limited. Reflectivity values are also expected to change during normal operation of the engine as random deposits on the optical surfaces are likely to promote diffuse, rather than specular, reflection. It should be recognized that the formation of fouling

on the optics, and its effect on coupling efficiency and reflectivity, is unpredictable; tests conducted as part of the IMAGER program showed that, although a general increase in attenuation over time should be expected, the rate and nature of this fouling do depend markedly upon the operating conditions of the engine. Given this lack of control over the coupling efficiency and reflectivity, reliance on them for suppression of interferometric noise would be unwise but an understanding of their influence is nonetheless useful. Reduction of back reflections elsewhere in the optical system does, however, provide an excellent means for the suppression of other etalons. Consequently, in common with other authors, we make use of Faraday isolators and angled physical contact (APC) connectors, the latter being far superior (>10dB) to standard physical contact (PC) types in this regard. The cosine term in equ. (4) can also be used to achieve interference reduction. If the cosine can be either forced to zero or made to cycle rapidly, such that its time average in the measurement bandwidth approaches zero, the effect of the etalon will be eliminated. The former approach is impractical for our purposes as the beam path length, and consequently τ, will change continuously as a result of thermal expansion and flexing during operation. Reduction of the time average of this cosine term forms the basis of the various jitter approaches that have been reported, e.g. Cassidy & Reid.[30] By modulating rapidly across one fringe spacing of the interference, the underlying absorption signal can be recovered accurately. This modulation is typically of lesser amplitude and higher frequency than any applied to permit detection using a lock-in amplifier, to which it may, or may not, be harmonically related. In our system, the free spectral range (FSR) of a typical combustion chamber etalon will be 0.017 nm (at 1700 nm) but significant variation will result from the diverse path lengths of the individual beams. Consequently, no attainable level of jitter will simultaneously

satisfy the requirement for all paths, which limits the usefulness of this technique where, as in our case, concurrent parallel measurements are required. Stewart *et al*[29] present a more detailed analysis, including both wavelength and amplitude modulation of the source, and show that, for a given etalon, *minimization* of the interference term can be achieved by appropriate selection of the wavelength modulation depth. This avoids the additional hardware complexity necessary for the introduction of jitter but the preceding comments regarding the lack of a globally ideal solution remain valid. Interestingly, they show that the region in which the highest signal to interferometric noise ratio (SNR_I) occurs also exhibits the greatest variability in that quantity, with respect to modulation index. Deeper modulation results in less optimal, but more stable, SNR_I performance. In our system, with its wide spread of FSR values, such deep modulation may offer a better *average* level of interferometric noise performance across all beams, whilst making full use of the available optical power. The last point is highly significant; even if a substantial decrease in modulation index did yield improved SNR_I, it would be detrimental to other aspects of the SNR, particularly once significant contamination of the collimators has occurred.

Other forms of optical noise result from the use of fiber optics but are exacerbated by the environment. Bend losses become a significant problem if they are modulated during operation, e.g. by flexing of the engine block, as this will give rise to signal artefacts at frequencies related to the engine cycle. Such artefacts can be very difficult to distinguish from real processes of interest. Modal noise is a further concern as engine vibrations provide a ready means for time-varying launch conditions into the receive fiber. Comparatively large detectors (0.3 mm diameter) are used, at the expense of slightly higher electronic noise, to ensure that the energy from

all modes is collected, although some residual effect will remain due to sensitivity variation across the detector. Cladding modes may also be influential; given the relatively short fiber lengths involved, an equilibrium mode distribution will not be achieved. The removal of high-order modes may be advantageous in some circumstances.

Overall, the optoelectronic design has to reconcile several, sometimes conflicting, requirements. Our first experiences of system operation on an engine suggest that optical noise can be suppressed sufficiently to permit imaging but that this requires careful design, especially with regard to fiber management. Interferometric noise proved less of a problem than had been expected from initial laboratory tests, probably due to the reduced coupling efficiency. High levels of noise were observed under operating conditions that resulted in substantial fiber movement (Figure 9). Such noise is likely to include modal, bending, and connector contributions but the generic solution, currently being implemented, is an increase in the level of environmental protection offered to the fibers. The optical power budget remains severely limited. As signal levels decline during operation, we anticipate that a point will be reached at which electronic noise replaces optical noise in limiting the SNR, despite the improvements that have been made in the former. Furthermore, this transition is unlikely to take place at the same rate for all measurement paths; the severity of fouling is expected to vary according to location in the combustion chamber so measures intended to improve the quality of data from one path may prove detrimental to that obtained from others. At first glance, such uncertainty seems to offer little rational basis for design but it should be recognized that variability is *inherent* in the target application; engine speeds, loads and temperatures all contribute to the rate and nature of the fouling, and engine management systems may impose

additional time-variation in operating conditions. The measurement is fundamentally parallel; by identifying and discounting those measures which cannot be relied upon to bring about *global* improvement, effort can be directed at others, such as receiver noise reduction, that offer more certain benefits.

Architecturally, the new design remains very similar to our first generation tomograph. It uses fiber-coupled diode lasers, of nominal wavelengths 1651 nm and 1700 nm. Modulation inputs to these lasers are provided by a 4-output direct digital synthesis (DDS) module (to be reported elsewhere) that offers good spectral-purity (>55dBc), together with highly flexible frequency (DC to 1 MHz), phase and amplitude. A commercially-available wavelength division multiplexer and 1 × 32 coupler connect these sources to the OPAL, via 9/125 single mode fiber. Multimode links return from the OPAL to a bank of photodiode receivers and dual lock-in amplifiers, which communicate with a data acquisition PC over a fast (>10 Mbyte/s) digital interface. The entire system has been designed to allow 8000 fps imaging using lasers modulated at nominal frequencies of 300 kHz and 500 kHz, although the actual operating frequencies are readily adjusted.

It should be noted that the use of an alternative approach, described by McNesby *et al*,[5] in which both laser sources are modulated at the same frequency but 180° out-of-phase would reduce the *overall* bandwidth requirement, as carrier separation would no longer be an issue. Any imbalance in the attenuation of the two beams gives rise to a periodic variation (at the modulation frequency) in the total intensity at the detector, which can be readily measured using a lock-in amplifier. This approach also halves the number of lock-in amplifiers required for demodulation but McNesby *et al* point out that adequate matching of the laser outputs is hard to achieve without the use of external electro-optic modulators. More significantly, for

our application, information about non-resonant attenuation, which we have shown to be of use in spray imaging, can only be obtained by examination of the unmodulated (near-DC) components of the received signal, which will be affected by thermal radiation reaching the detector, system offsets, and 1/f noise. Overall, we continue to believe that accurate demodulation of the attenuation at *both* wavelengths is of sufficient importance to justify the additional hardware complexity involved in a dual-carrier scheme.

3.4 Example results from single-channel studies

The 3-channel system was tested on an otherwise standard 2.0 liter 4-cylinder port-fuel-injected gasoline engine, complete with its normal electronic control unit (ECU). Engine speed was controlled by the dynamometer and the load was adjusted by varying the throttle position. The engine was run on a reference fuel (ISOPAR C - similar to ULG but less prone to carbon deposition) to minimize fouling of the cylinder-wall optics. The engine was fired as it would be in normal operation, under ECU control. Instantaneous cylinder pressure data were obtained from an in-cylinder pressure transducer within the spark plug, which permits the calculation of the PCI from the measured attenuation values, for a given path. Measurements were made at several engine speeds (1000, 1500, 2000 rpm) and for a range of moderate applied loads (0, 1, 2, 3 bar brake mean effective pressure [BMEP]). The highest load-speed combination studied is equivalent to around 50 mph up a modest incline. Under such conditions, a relatively small amount of fuel will be present, although this will increase with load. The actual spatial distribution of fuel within the combustion chamber is, of course, unknown but the choice of an essentially diametric measurement path should ensure that the lasers traverse the fuel plume at some point.

Although the intrinsic signal-to-noise behavior of the system is good, the measurements obtained require additional processing to render them useful, due to other effects, associated with the engine. Firstly, engine operation is rarely completely stable; any single cycle may be atypical. Therefore, in the analysis presented here, a small number of cycles (usually around 25) are averaged to avoid misleading results. Secondly, variations not associated with the fuel, but nevertheless synchronous with the engine cycle, may be present, e.g. the effect of lubricant films. Comparison of fuelled and non-fuelled cycles is helpful in the detection of effects of this type. Finally, contamination of the lenses, e.g. by combustion products, creates variation in signal levels on a timescale much longer than the rotational period of the engine. Dynamic referencing of the data to a point late in the exhaust stroke (minimum fuel concentration) is used to overcome this. Together, these three measures permit the extraction of useful information from the complex raw measurement data, as evidenced by the results that follow. Other authors in the engine R&D community have applied similar procedures, e.g. Skippon *et al*.[9]

Processing the ratio of received intensity at 1700 nm to received intensity at 1550 nm in the above manner yielded normalized ratio values. Figure 10 shows the variation of these values with crank angle for four different load conditions, at 2000 rpm. The compression stroke is shown, from the time when the inlet valve ceases to obstruct the beam path to the earliest position at which ignition may occur, approximately 30° before TDC. The uppermost bold trace shows data obtained for operation without additional load. The next trace down (light line) is for a load of 1 bar BMEP. The lower bold and light traces correspond to loads of 2 and 3 bar BMEP, respectively. Neither the total fuel input during any given cycle nor its spatial distribution is known but a strong correlation must exist between the average fuel

concentration and the work being done against the applied load. The progressive decrease in ratio observed with increasing load is therefore in agreement with expectation. Furthermore, the magnitude of the change is broadly consistent with earlier absorption measurements made on similar fuels (unleaded gasoline and iso-octane) by Carey.[12] The presence of ratio values greater than unity probably results from the non-ideal reference strategy adopted, i.e. significant amounts of unburned HC are still present when the reference is taken during the exhaust stroke. This may be exacerbated by the use of ISOPAR C fuel, which is believed to be slower burning than ULG. The ECU was not calibrated for this fuel and some reduction in engine performance was observed. All four traces show the expected decrease in ratio as the engine approaches TDC (i.e. maximum compression), due to the increase in the volumetric density of the absorbing species, which more than offsets the modest expected decrease in the extinction coefficient with increase in pressure, as discussed in Section 1. Overall, good agreement with expected trends is evident, although the difficulty of validating system performance, in the absence of a known gas distribution, is obvious.

3.5 Current activity – full in-cylinder optical tomography

A new OPAL, featuring around 30 measurement paths, is presently being constructed to permit tomographic imaging of in-cylinder HC distributions. This will use essentially the same collimator design and constructional methods as the 3-channel version described in Section 3.2. Candidate topologies, based on what is possible within constraints imposed by the mechanical integrity and functionality of the engine, have been assessed (by simulation) to gauge their effectiveness. Simply maximizing the *number* of measurement paths is unlikely to yield the best solution.

This typically results in the close packing of collimators, which tends to create groups of closely-spaced and essentially parallel beams, which offer poor angular sampling of the measurement space. The optimization of the measurement grid for the new OPAL has proved to be a challenging task, with little precedent in existing literature. Establishing design rules, or at least principles, for this process is important if the system is to be applied to other engine types, with different inherent constraints. Once again, clear differences are evident between existing perspectives on best or normal practice, as derived from laboratory studies, and the demands of real-world applications. Assembly of the new OPAL, whilst undeniably demanding, relies on methods devised and tested during construction of the 3-channel version and is, therefore, not expected to require significant additional development effort.

Extension of the electronic systems used in our most recent tests to support a high channel-count involves more than mere replication of the basic photodiode receiver and signal recovery elements. At 8000 fps, data must be streamed from the 64 lock-in amplifiers used for demodulation at total rates in excess of 10^6 bytes / second. Even higher rates are foreseeable during spray imaging. A highly-parallel data acquisition architecture is being developed to address this need, which will permit data to be acquired at up to 10^7 bytes /second, allowing scope for increases in frame rate or channel-count in future versions of the system.

4. Discussion and Conclusions

CST has the potential to be a valuable tool in the monitoring of many industrial processes. However, despite successful proof-of-principle studies by several authors, little development into practical instrumentation has taken place. The authors believe that the reasons for this *do not lie in the fundamental capabilities of CST* as it undeniably possesses many desirable attributes for a process monitoring technique; it

offers fast, minimally-invasive, chemically selective measurement, and can be implemented in hostile environments (in terms of pressure, temperature, electromagnetic interference, vibration) as well as those requiring intrinsic safety. Nor is cost prohibitive; diode lasers suitable for sensing many species now cost less than $10K. Instead, in our view, it is the *technological challenge of its implementation* that forms a barrier to widespread acceptance. To address this issue we have sought to demonstrate here not just a technique in principle but also its development into a practical instrument. HC imaging within a vehicle engine embodies many difficulties that will be encountered in other applications of CST, including a very limited optical power budget, constraints upon the number and distribution of measurement paths, harsh environmental conditions both within and around the process vessel, and various sources of optical and electronic noise. It is hoped that, on examining the manner in which this example has evolved from the laboratory bench towards practical application, other researchers will be encouraged to pursue potential applications of CST. The overall methodology, of absorption selection and characterization, followed by pilot studies, and finally implementation, has much to recommend it but constraints upon the form of the eventual solution should be identified early and incorporated within the pilot stages, if it is to be effective.

Inevitably, the most appropriate instrument architecture will vary, depending upon the requirements of the individual application. In our case, the overwhelming demand for temporal resolution dictates the use of simultaneous launch and receive on all channels. This, together with the broad, unstructured form of the target absorption feature renders inapplicable many of the techniques reported in the literature for enhancing the sensitivity of near-IR absorption measurements. Other instances of

CST may, of course, be able to exploit such techniques and/or alternative architectures, e.g. to achieve the sensitivity required for the imaging of minor species.

We have previously developed[2,3] the principles of HC imaging by near-IR absorption at 1700 nm. In this paper, we have presented further results from that work, and have shown how acceptable images can be obtained from small numbers of measurements; we have also shown that from such a foundation it is possible to develop measurement solutions, appropriate for studies of fuel distribution within the combustion chamber of an essentially standard vehicle engine. A program of mechanical, optical, and electronic design and testing has underpinned the transfer of the technique from the laboratory into the engine environment. In particular, significant effort has gone into the design of the collimators and the development of a workable procedure by which pairs thereof may be aligned within the OPAL. Other issues, such as sealing integrity, that have the potential to interfere with the measurement process have been successfully addressed in the reduced channel-count prototype. The basic durability of the collimators has also been established during these pilot studies. Cross-cylinder near-infrared attenuation measurement has been shown to be possible in a running multi-cylinder production engine, demonstrating beyond doubt the feasibility of performing chemical species tomography in such an environment. Encouragingly, it has proved possible to maintain uninterrupted optical access to the cylinder over several hours of engine operation, which is easily sufficient to permit the study of many phenomena of interest, e.g. cold starting. The DWR technique continues to prove effective in rejecting unwanted sources of signal variation, despite the increased severity of these effects, as compared to previous work on laboratory phantoms and research engines. After suitable processing, the

results obtained exhibit variations with applied load and crank angle that are consistent with expectation.

The optical design of our most recent system has, inevitably, been heavily influenced by the constraints of the production engine environment but careful engineering has allowed us to attain an acceptable level of performance. Given suitable fibers, the approach developed for IMAGER may ultimately offer a better route to mid-IR measurement within a combustion chamber than the use of sapphire cylinders, which have some limitations when subject to thermal transients.[31] Implementation of an OPAL featuring around 30 measurement paths remains a substantial engineering challenge, however. Key elements of the new system's electronic design, including the photodiode receiver and lock-in amplifiers, have been subjected to extensive testing, both in the laboratory and at a commercial engine-test facility. Despite supporting operation at higher frequencies than previously, these offer a significant reduction in electronic noise, as compared to our earlier system, to support the required increase in imaging rate. The data obtained in the pilot study are believed to be the first published optical absorption measurements, at any wavelength, to be made across a combustion chamber of a multi-cylinder engine. These data are of sufficient quality that, if a similar level of performance could be achieved for all measurement paths of the final (≈ 30 channel) OPAL, 8000 fps imaging would be possible, with acceptable resolution in HC concentration. Some further improvement in the SNR of the individual path concentration measurements is expected once the increased modulation frequencies and reduced wavelength spacing are implemented. Additional engine testing, using the 3-channel OPAL, will be carried out to quantify the performance achievable with these measures in place.

Although there has been significant progress in our work concerning the use of image reconstruction algorithms for a small number of PCI measurements, even when they are taken from an irregular measurement array, it is important to recognise that these are aspects that are still relatively unexplored for 'hard-field' tomography. The expression 'hard-field' applies to tomographic modalities where the PCI or equivalent signal only depends on the material that lies in a known path from excitation source to detector, to first order. Electrical Tomography (ET), on the other hand, yields a 'soft-field' signal in that every measurement is dependent on the electrical properties of every part of the measurement subject. ET is now well developed[32] and usually yields only a few dozen measurements. Hence, image reconstruction techniques taken from that modality may be usefully exploited for CST in the future. For now, it is of the utmost importance that, in viewing the images in this paper, the reader consciously bears in mind the spatial resolution limitations and the artefacts discussed in Section 3.1. From experience of the development of ET, it can be confidently expected that further research will improve the robustness of the image reconstruction algorithms for CST, and the capability to design optimally the array of beam paths for any given application.

From our recent experience of operating the system with a 3-channel OPAL, it appears that the prospects for tomographic imaging of in-cylinder fuel-vapour distributions in a production IC engine, using an extended version of this same system, are extremely good. The authors wish to acknowledge the financial support of the Engineering & Physical Sciences Research Council and the Department of Trade & Industry (UK). Particular thanks go to Steve Gratze (DTI) for his valued input.

References

1. R. J. Santoro, H. G. Semerjian, P. J. Emmerman and R. Goulard, "Optical tomography for flow field diagnostics," Int. J. Heat Mass Transfer, **24,** 1139-1150 (1981)

2. S. J. Carey, H. McCann, F. P. Hindle, K. B. Ozanyan, D. E. Winterbone and E. Clough, "Chemical species tomography by near infra-red absorption," Chem. Eng. J. **77**, 111-118 (2000).

3. F. P. Hindle, S. J. Carey, K. B. Ozanyan, D. E. Winterbone, E. Clough and H. McCann, "Measurement of gaseous hydrocarbon distribution by a near-infrared absorption tomography system," J. Electronic Imaging **10**(3), 593-600 (2001).

4. K. Salem, E. Tsotsas and D. Mewes, "Tomographic measurements of breakthrough in a packed bed adsorber," Chem. Eng. Sci. **60**(2), 517-522 (2005).

5. K. L. McNesby, R. T. Wainner, R. G. Daniel, R. R. Skaggs, J. B. Morris, A. W. Miziolek, W. M. Jackson, and I. A. McLaren, "Detection and measurement of middle-distillate fuel vapors by use of tunable diode lasers," Applied Optics **46**, 840-845 (2001)

6. B. Culshaw, G. Stewart, F. Dong, C. Tandy and D. Moodie, "Fibre optic techniques for remote spectroscopic methane detection – from concept to system realization," Sensors and Actuators B **51**, 25-37 (1998).

7. P. A. Martin, "Near-infrared diode laser spectroscopy in chemical process and environmental air monitoring," Chem. Soc. Rev. **31**, 201-210 (2002).

8. M. G. Allen, "Diode laser absorption sensors for gas-dynamic and combustion flows," Meas. Sci. Technol. **9**, 545-562 (1998).

9. S. M. Skippon, S. R. Nattrass, J. S. Kitching, L. Hardiman and H. Millar, "Effects of fuel composition on in-cylinder air/fuel ratio during fuelling transients in an SI

engine, measured using differential infrared absorption," SAE Technical Paper No. 961204 (Society of Automotive Engineers Inc., Pennsylvania, 1996).

10. A.E.M. Barrag and B. Lawton, "Computer optical tomography in the study of internal combustion engine soot concentration," 26th international symposium, Automotive technology and automation, Vol.: "The motor vehicle and the environment – demands of the nineties and beyond", Aachen (1993).

11. H. Philipp, A. Plimon, G. Fernitz, A. Hirsch, G. Fraidl and E. Winklhofer, "A tomographic camera system for combustion diagnostics in SI engines," SAE Technical Paper No. 950681 (Society of Automotive Engineers Inc., Pennsylvania, 1995).

12. S. J. Carey, *Chemical Species Tomography by Near Infrared Absorption* (Ph. D. thesis, UMIST, UK, 2001).

13. L. S. Rothman, C. P. Rinsland, A. Goldman, S. T. Massie, D. P. Edwards, J-M. Flaud, A. Perrin, C. Camy-Perrey, V. Dana, J-Y. Mandin, J. Schroeder, A. McCann, R. R. Gamache, R. B. Wattsin, K. Yoshino, K. V. Chance, K. W. Juck, L. R. Brown, V. Nemtchechin and P. Varanasi, "The HITRAN molecular spectroscopic database and HAWKS (HITRAN atmospheric workstation): 1996 edition," J. Quant. Spect. And Radiative Transfer **60**(5), 665-710 (1998).

14. F. Natterer, *The Mathematics of Computerised Tomography* (Wiley, Chichester, 1986).

15. R. Gordon, R. Bender and G. T. Hermann, "Algebraic reconstruction techniques (ART) for 3-dimensional electron microscopy and X-ray photography," J. Theor. Biol., **29** (3), 471-481 (1970).

16. F. P. Hindle, S. J. Carey, K. B. Ozanyan, D. E. Winterbone, E. Clough and H. McCann, "Near infra-red chemical species tomography of sprays of volatile hydrocarbons," Technisches Messen **69**(7-8), 352-357 (2002).

17. M. Bertero and P. Boccacci, *Introduction to Inverse Problems in Imaging* (IOP Publishing, Bristol, 1998).

18. A. H. Andersen, "Algebraic reconstruction in CT from limited views," IEEE Trans. Med. Imaging **8**(1), 50-55 (1989).

19. D. Verhoeven, "Limited data computed tomography algorithms for physical sciences," Applied Optics **32**(20), 3736-3754 (1993).

20. J. Feng, "Reconstruction in tomography from severe incomplete projection data using multiresolution analysis and optimization," in *Proceedings of 7th IEEE Digital Signal Processing Workshop* (Institute of Electrical and Electronics Engineers, New York, 1996), pp. 133-136.

21. S. H. Wong and S. F. Yau, "A linear sinogram extrapolator for limited angle tomography," in *Proc. Third International Conf. on Signal Proc.* (Institute of Electrical and Electronics Engineers, New York, 1996), pp. 386-389.

22. C. A. Garcia-Stewart, N. Polydorides, K. B. Ozanyan and H. McCann, "Image reconstruction algorithms for high-speed chemical species tomography," in *Proceedings of the 3rd World Congress on Industrial Process Tomography*, T. Dyakowski and A. Kantzas, ed. (University of Leeds, UK, 2003), pp. 80-85.

23. S. Singh, K. Muralidhar and P. Munshi, "Image reconstruction from incomplete projection data using combined ART-CBP algorithm," Def. Sci. J. **52**, 303-316 (2002).

24. T. S. Pan and A. E. Yagle, “Acceleration of Landweber-type algorithms by suppression of projection on the maximum singular vector,” IEEE Trans. Med. Imaging **11**, 479-487 (1992).

25. W. Q. Yang, D. M. Spink, T. A. York and H. McCann, “An image-reconstruction algorithm based on Landweber’s iteration method for electrical-capacitance tomography,” Meas. Sci. Technol. **10**, 1065-1069 (1999).

26. P. Wright, K. B. Ozanyan, S. C. Murray, T. J. Litt, S. Pegrum, S. Colbourne, and H. McCann, “First optical attenuation measurements across the cylinder of a production IC engine,” in *Proceedings of the 4th World Congress on Industrial Process Tomography* (to be published).

27. P. Wright, K. B. Ozanyan, S. J. Carey and H. McCann, “Design of High-Performance Photodiode Receivers for Optical Tomography,” IEEE Sensors **5**(2), (2005).

28. C. K. Kirkendall and A. Dandridge, “Overview of high performance fibre-optic sensing,” J. Phys. D: Appl. Phys. **37**, R197-R216 (2004).

29. G. Stewart, A. Mencaglia, W. Philp and W. Jin, “Interferometric signals in fiber optic methane sensors with wavelength modulation of the DFB laser source,” J. Lightwave Tech. **16**(1), 43-53 (1998).

30. D.T. Cassidy and J. Reid, “Harmonic detection with tuneable diode lasers – two-tone modulation,” Appl. Phys. B **29**, 279-285 (1982).

31. R. M. Richman and W. C. Reynolds, “The development of a transparent cylinder engine for piston engine fluid mechanics research,” SAE Technical Paper No. 840379 (Society of Automotive Engineers Inc., Pennsylvania, 1984).

32. B. S. Hoyle, H. McCann and D. M. Scott, “Process Tomography”, in D. M. Scott and H. McCann (editors), “Process Imaging for Automatic Control”, Chapman & Hall/CRC Press, Boca Raton (2005), chap. 4

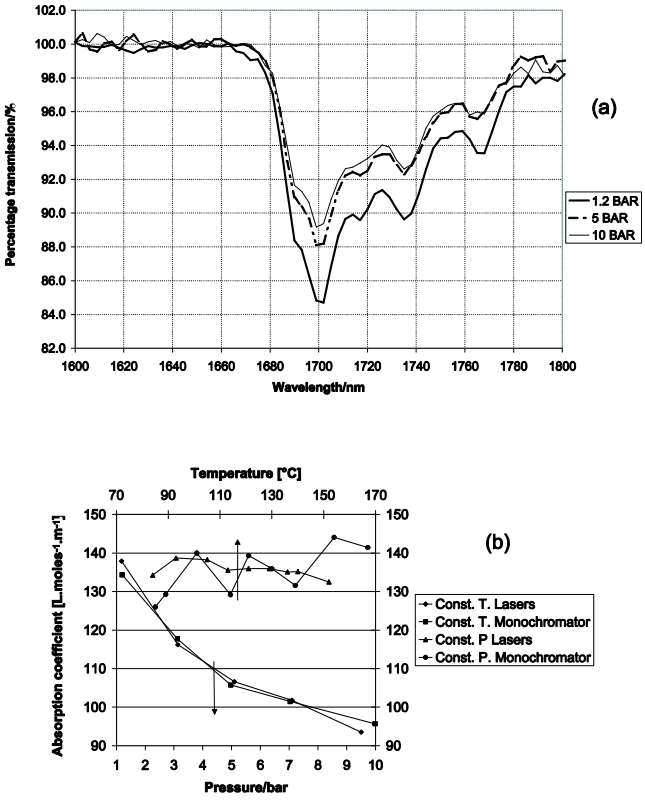

Figure 1: (a) Effect of pressure on iso-octane transmission at constant temperature of 150°C. Concentration 0.0073 mol/liter; Source Bandwidth 5 nm. (b) Difference in absorption coefficient as measured with lasers (1700 nm compared to 1550 nm) and a monochromator (1700 nm compared to 1650 nm) with changing pressure (at constant 150°C) and changing temperature (at 1.2 bar)

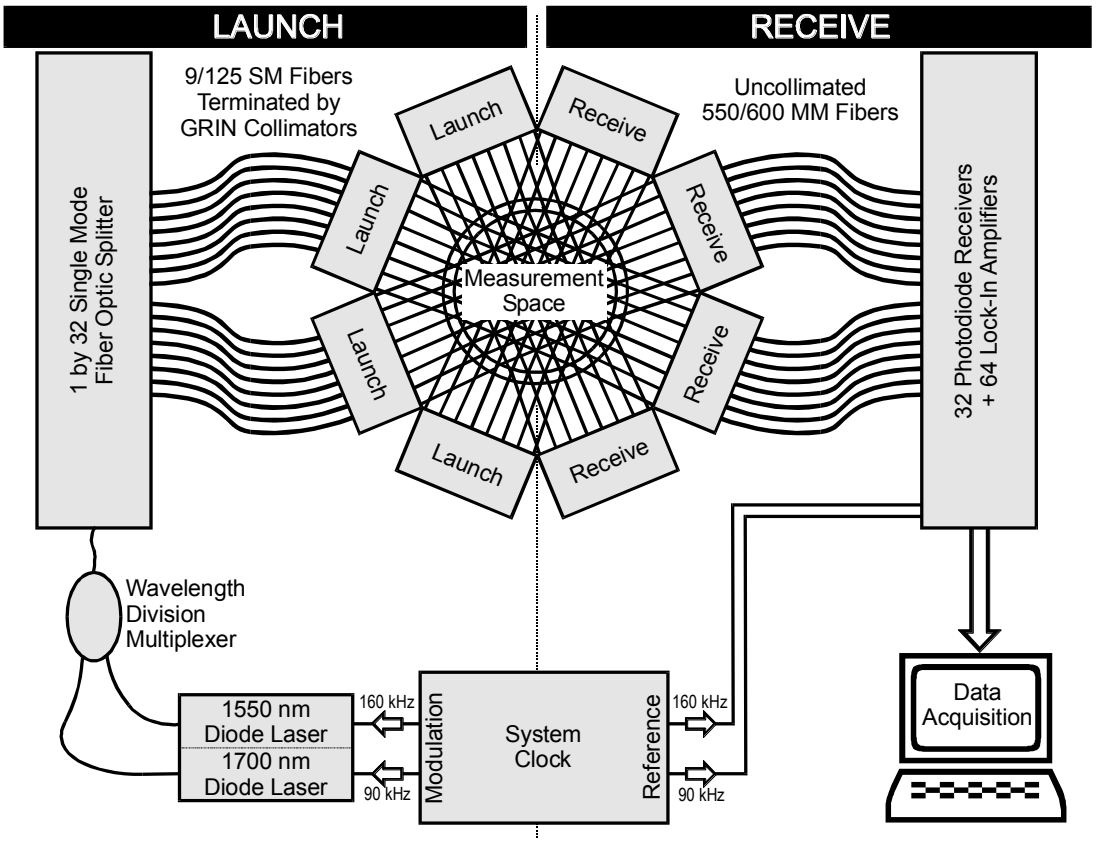

Figure 2 – Schematic overview of first-generation chemical species tomography system.

Figure 3 – Laboratory implementation of simulated in-cylinder conditions. The silica-walled pressure vessel (centre of picture) is shown configured for liquid fuel injection. Inlet and outlet hoses allow for purging and pressurization of the chamber with air or nitrogen. A heating element in the base of the chamber controls the temperature. The outer support ring is used for mounting and alignment of the 64 fiber optic elements, in 4 projections of 8 beams each.

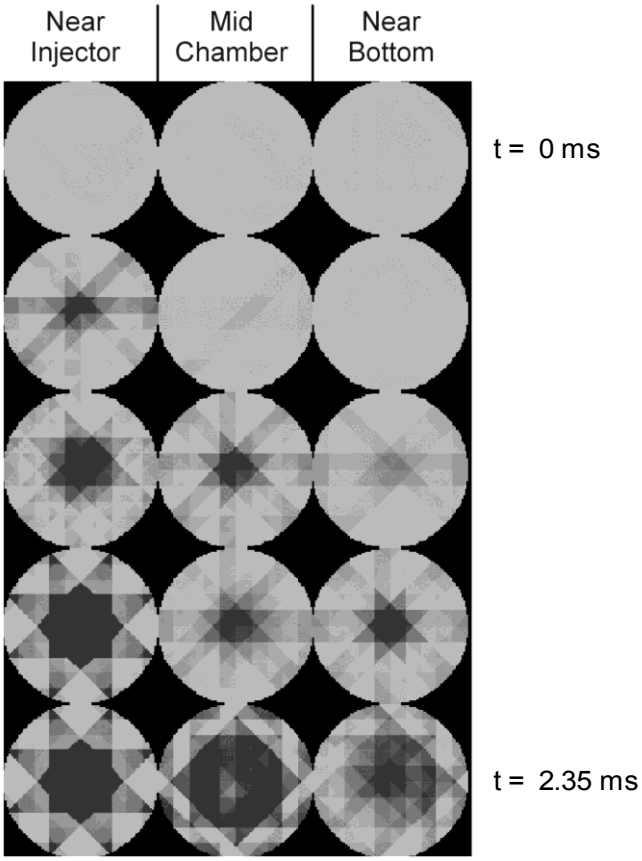

Figure 4 - Reconstruction of 1550nm data from 0.0 to 2.35 ms (darker regions correspond to higher levels of attenuation). The fuel injections used in this test were generated with the assistance of Dr. G. Wigley (Loughborough University) and Lotus Engineering.

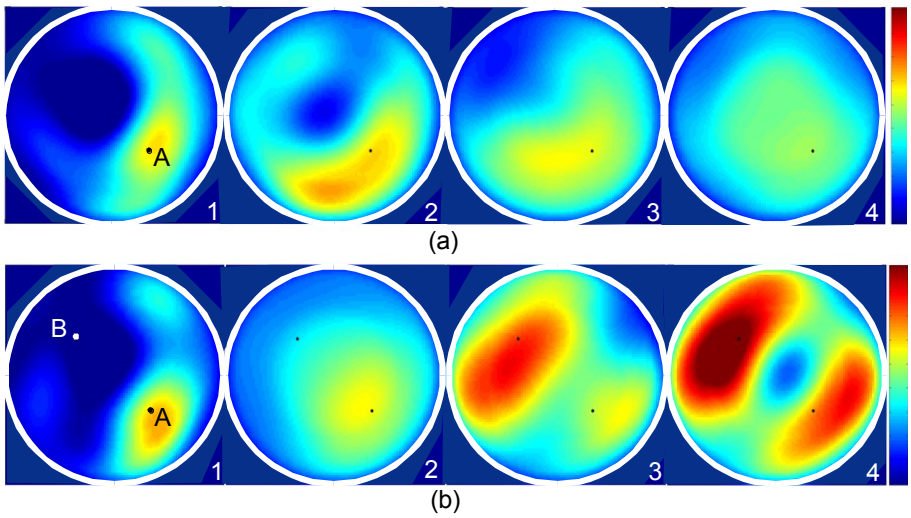

Figure 5: (a) Reconstructed images of a 10 ms low-pressure propane injection into air in a cylindrical engine simulator. The images shown correspond to times 30.6 ms, 51.2 ms, 98.5 ms and 145.0 ms after the start of the pulse to activate the injection. The centre of the injection pipe is shown by a dot. The units of propane concentration are arbitrary but the color bar represents a linear scale. (b) Reconstructed images of two sequential 10 ms low-pressure propane injections into air in a cylindrical engine simulator, with a 100 ms delay between injections. The images shown correspond to times 28.8 ms, 98.8 ms, 136.5 ms and 145.0 ms after the start of the pulse to activate the first injection. The centre of each injection pipe is shown by a dot. The units of propane concentration are arbitrary but the color bar represents a linear scale.

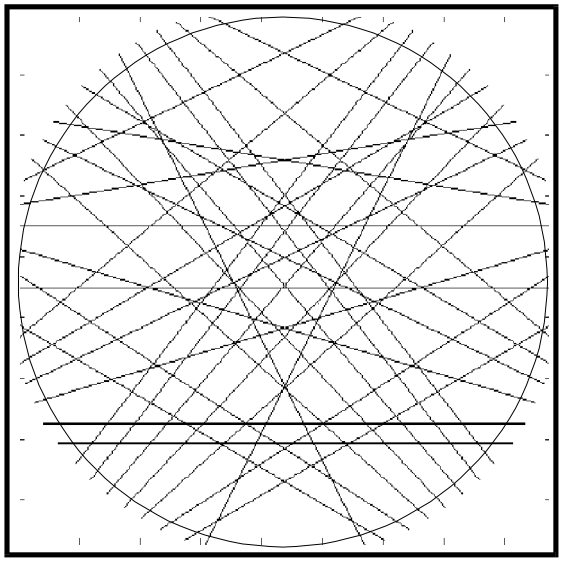

Figure 6: Candidate 32-beam array used in simulation studies. The absence of beams in the region at the bottom-centre of the array is due to the proximity of the adjacent cylinder.

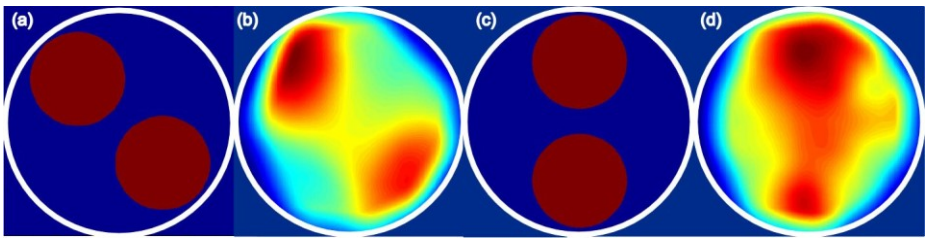

Figure 7 - Illustrations of aspects of the performance of the irregular measurement array in Figure 6, using the reconstruction technique given in the text. Figure 7(a) shows a simulated phantom distribution consisting of two circular high-concentration clouds, and Figure 7(b) shows the reconstructed distribution for that phantom. Figure 7(c) shows the phantom distribution following a 45 degree rotation and 7(d) shows the corresponding reconstructed distribution.

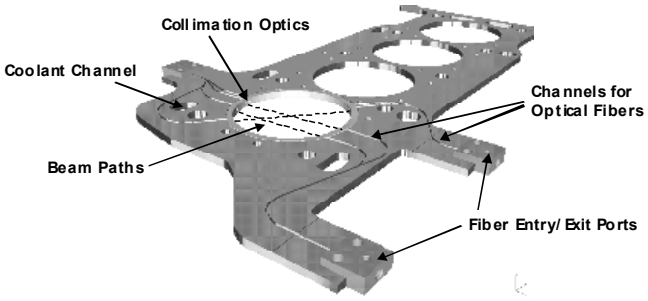

Figure 8: The 3-channel optical access layer (OPAL)

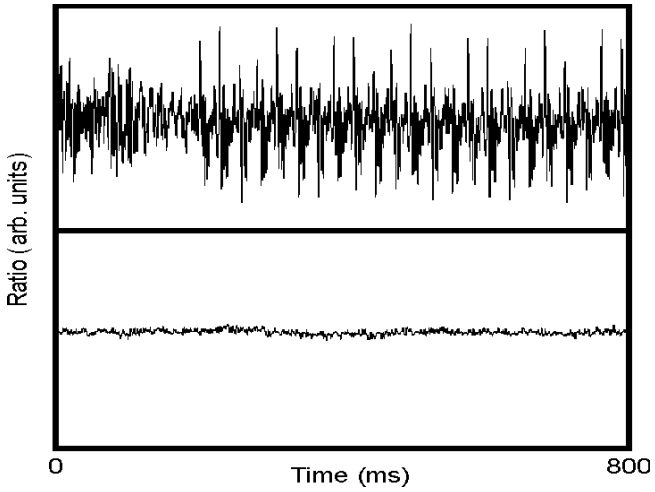

Figure 9 – Effect of fiber vibration on noise levels. The upper panel shows the noise level achieved in the ratio using standard 3 mm jacketed patchcords for optical interconnects (excluding those on the engine itself) exposed to the engine test cell environment. The lower panel (same scale) shows 'laboratory' performance using the same optical setup. The SNR degradation is around 20 dB, highlighting the importance of effective environmental protection of the fibers.

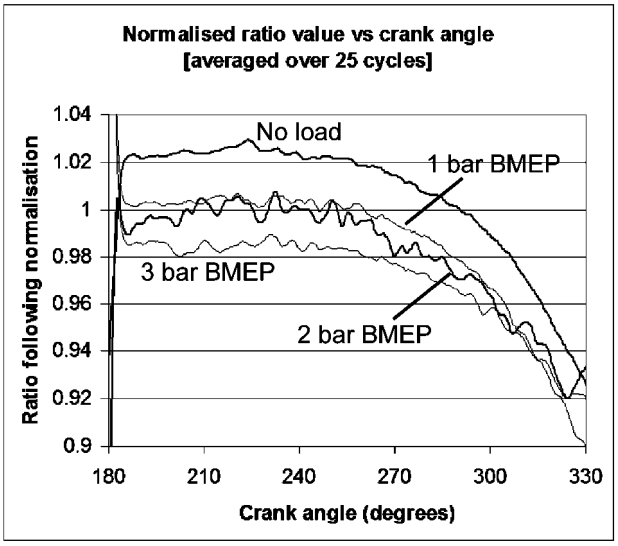

Figure 10: Example results from an engine running on ISOPAR C fuel under four levels of load